

Journal of Stress Analysis

Vol. 8, No. 2, 2023-24, 41-50



ORIGINAL RESEARCH PAPER

The Effect of ECAP Process on the Microstructure and Mechanical Properties of AISI 1020 Plain Carbon Steel

Kaveh Hajizadeh*

Department of Mining and Materials, Faculty of Engineering, Urmia University of Technology, Urmia, Iran.

Article info

Article history: Received 10 November 2023 Received in revised form 24 January 2024 Accepted 22 February 2024

Keywords: Equal channel angular pressing AISI 1020 Ultrafine-grained materials XRD TEM

Abstract

In the present study, the equal channel angular pressing (ECAP) was applied on AISI 1020 plain carbon steel to refine the grain size down to the submicrometer range. ECAP was conducted up to 10 passes at 300 $^{\circ}\mathrm{C}$ in a die with a channel angle of 105°. The microstructure before and after ECAP was observed in two different scales using a light microscope and a transmission electron microscope (TEM). Evaluation of mechanical properties was carried out by tensile tests and microhardness measurements. The results indicate that by applying 10 passes of ECAP, an ultrafine-grained microstructure with a mixture of equiaxed and elongated grains with an average grain size and width of 320 and 270 nm, respectively, is formed in the steel. In addition, the analysis of the X-ray peak profiles of the ECAP-ed samples shows that inside the grains, there are finer microstructural components such as dislocation cells/subgrains. The average size of these components was measured at \sim 143nm. In terms of mechanical properties, it was proven that ECAP is very effective in improving the strength and hardness of the steel. It causes a three times growth in yield strength from 280MPa to 1100MPa and a 1.67 times increase in hardness from 125 to 395 Vickers. At the same time, the studied material showed an acceptable ductility of $\varepsilon_f = 14.8\%$ at these high strength levels. These promising mechanical properties was discussed in terms of characteristics of the ECAP-produced microstructure: extremely fine grains/subgrains, and increased dislocation density.

1. Introduction

AISI 1020 is one of the most widely used plain carbon steels, the distinctive features of which such as high machinability, good weldability, and enough ductility make it usable in various applications [1]. Automotive, truck, and agricultural components such as axles, bolts, shafts, light gear, spindle, seat brackets, and motor-brake wheels are just examples of the use of this steel [1]. However, the low carbon concentration (about 0.2%) and the absence of alloying elements make this steel respond poorly to common

hardening treatments such as quenching and tempering or nitriding [2]. Therefore, steel factories employ the mechanism of work hardening to increase the strength of this steel and offer some types with higher strength, called cold worked type, to the market [3]. Increasing the dislocation density of the microstructure through cold working, although strengthening the steel, makes a significant reduction in ductility [4, 5]. In comparison with the cold worked state, ultrafine-grained/nanocrystalline microstructures obtained from methods of severe plastic deformation (SPD) not only lead to a substantial increase in material's strength,

*Corresponding author: K. Hajizadeh (Associate Professor)

E-mail address: kaveh.hajizadeh@uut.ac.ir

doi 10.22084/JRSTAN.2024.28243.1248

ISSN: 2588-2597



Copyright ©2023 The Authors. Published by Bu-Ali Sina University. This work is licensed under a Creative Commons Attribution-NonCommercial 4.0 International license (https://creativecommons.org/licenses/by-nc/4.0/). Non-commercial uses of the work are permitted, provided the original work is properly cited.

but also they show better ductility than the cold work state [6]. Therefore, SPD processing provides a suitable opportunity to bring about a good combination of high strength and tolerable ductility in weak plain carbon steels such as AISI 1020 and consequently expands their range of applications.

A review of the literature shows that in many of previous works [7-12], equal channel angular pressing (ECAP) was utilized on the grain refinement of low carbon steels. In this regard, Shin et al. [7, 8] conducted ECAP using route C (rotation of 180° between two consecutive passes) by a die with a channel angle of 90° on a 0.15wt% C carbon steel at 350°C up to an effective strain of ~ 4 and reported ferrite grain refinement from 30 to $0.2-0.3\mu m$. The obtained microstructure led to a substantial increase of ultimate tensile strength (UTS) from 480 to 943MPa with reasonable total elongation of 11%. Fukuda et al. [9] refined the Fe-0.08 wt% C to the grain size of $\sim 0.2 \mu m$ by room temperature ECAP with a 90° die using route B_C (rotation by 90° in the same direction between two consecutive passes) for an equivalent strain of 3. The UTS increased to over 800MPa and the material exhibited an extensive region of strain hardening and high elongation to failure, approaching $\sim 40\%$. Successful room temperature ECAP of low carbon steels using dies with channel angle of 90° can only be carried out by two or three passes. Applying more passes often causes samples to fail. On the other hand, imparting an accumulated strain of ~ 3 to the material is not sufficient to produce an ultrafine-grained (UFG) structure. For this purpose, generally, an accumulated strain over $\sim 4-7$ is required [4].

One solution to improve the workability of samples during ECAP is to use high processing temperatures. Shin et al. [7, 8] used this strategy and succeeded in ECAP Fe-0.15wt% C safely up to four passes. It should be noted that although the high processing temperature improves the workability, it accelerates the occurrence of recovery and grain growth phenomena, leading to less microstructure refinement [4, 5]. The channel angle of ECAP die is an important factor dictating the magnitude of shear stresses generated at the intersection of two channels [5]. The larger angles make the lower amounts of the shear stress imposed on the sample [5]. On the other hand, according to finite element simulation results, when a larger channel angle is used, the plastic deformation region at the intersection of two channels expands instead of concentration in a narrow plane [13]. Thus, it can be expected that by using ECAP dies with channel angles larger than 90°, the failure of carbon steel billets will delay and shift to a larger number of ECAP passes [14]. By improving the workability of the billets due to the use of a larger channel angle, it is possible to impart high strain levels to the material and fabricate a fully refined grain structure.

For the first time, an ECAP die with a channel angle of $\Phi=105^\circ$ was used for processing a low carbon steel in this research. The billets were successfully ECA pressed up to 10 passes at 300°C using this die. The final microstructure and the evolution of tensile properties and hardness of the processed material were investigated.

2. Experimental Procedure

2.1. Materials and Experiments

The metal investigated in this study was AISI 1020 plain carbon steel. A bar with a diameter of 20mm and a length of 80cm was provided from the market, and its chemical analysis was determined using an optical emission spectrometer (Table 1). Small pieces of 8 cm were prepared from the bar, and then in order to remove the previous thermal and mechanical regime, annealing treatment was applied on them. Annealing was performed at 900°C for one hour, after which the samples were cooled to room temperature inside the furnace. In the next step, suitable ECAP samples with a diameter of 14.5mm and a length of 70mm were prepared through machining. ECAP was performed in a self-heating die with a channel angle of $\Phi=105^{\circ}$ and a corner angle of $\psi=20^{\circ}$, which was capable of heating the sample up to 400°C. The die was heated through six heating elements inserted into the drilled holes inside the die. More information about the design of the die and its accessories can be found elsewhere [14].

Table 1 Chemical composition of AISI 1020 plain carbon steel used in the present study.

С	Si	Mn	Ni	Cr	Р	S	Fe
0.19	0.35	0.62	0.24	0.15	0.04	0.045	Balance

ECAP was conducted at 300°C up to 10 passes using route B_C . In this route, the sample was rotated 90 around its longitudinal axis between two consecutive passes and the direction of rotation remained unchanged until the end of the process [5]. To reduce friction, a lubricant mixture containing graphite powder (50% in weight), molybdenum disulfide powder (25% in weight), and ordinary grease (25% in weight) was used [14]. The die used in this study, based on its Φ and ψ angles, imposed an equivalent plastic strain of $\varepsilon_{VM} = 0.8$ on each pass [5]. Therefore, during 10 passes ECAP by this die, a total strain of $\varepsilon_{VM} = 8$ was imparted to the sample. The microstructure observations were done in two length scales using a Meiji MT7100 light microscope and a JEOL JEM 1200EX transmission electron microscope (TEM) with a working voltage of 120kV. Light microscope samples were prepared by the standard method, and then etched in a nital solution containing 2% by volume of nitric acid in alcohol. TEM samples were cut from the side plane of the ECAP-ed bars, that is, the plane parallel to the longitudinal direction of the bars. These samples were first thinned mechanically by sanding and then by electrolytic polishing. The latter was done inside a jet polishing machine at ambient temperature using a solution containing 10% by volume of $\mathrm{HClO_4}$ in ethanol at an applied voltage of 15V. To evaluate the mechanical properties, microhardness measurements and tensile testing were employed. Tensile testing was carried out in an MTS 810 universal hydraulic servo-controlled machine with an initial strain rate of $5\times10^{-4}\mathrm{s}^{-1}$. For each processing condition, three specimens were subjected to tensile testing to ensure the reproducibility of the results.

In this work, in addition to microscopic observations, X-ray diffraction (XRD) was also used to study the microstructure. Diffraction patterns were recorded in a Bruker AXS D8-ADVANCE model diffractometer using Cu $K\alpha$ radiation with a wavelength of 1.5406 Angstroms and a scan speed of 0.005°/s. A well-annealed coarse-grained sample was employed as the standard specimen to correct the instrument-related broadening.

2.2. The Warren-Averbach Analysis

It is well known that [15, 16] applying plastic deformation to a metal leads to the broadening of the recorded X-ray peak profiles but decreases their intensity. This behavior is attributed to the smaller grain/subgrain size of the deformed microstructure and the lattice strains induced by dislocations with high density [16]. Methods of Williamson-Hall and Warren-Averbach are the two standard procedures by which microstructural parameters such as subgrain/dislocation cell size and dislocation density could be quantitatively estimated by the peak profile analysis [15, 17]. In this research, Warren-Averbach method was used. The analysis steps were as follows: first the background and the peaks related to $K\alpha_2$ radiation were removed from the initial diffraction pattern recorded by the diffractometer. Then the intensity of each peak was plotted again; however, this time as a function of the diffraction vector length (K) instead of the diffraction angle (2θ) . In Warren-Averbach method, two peaks of the same family are used for analysis. For the steel used in this study, the peaks related to plane of (110) and (220) were utilized. X-ray diffraction peak profiles could be approximated in shape with good accuracy using a combination of the Gaussian and Lorentzian functions [18].

For each of the two peaks of the same family, two curves were fitted with Gaussian and Lorentzian functions. In the next step, the Fourier transformation was taken from the resulting relationships for these peaks. After that, for different values of the Fourier variable (L), the value of the real Fourier coefficient (A(L)) was

calculated and plotted versus L for both peaks. Then, for a particular magnitude of the Fourier variable, the A(L) values were recorded on both peaks, and then the Naperian logarithm of these values were drawn in terms of the square of the diffraction vector length (K^2) of the peaks. According to the Warren-Averbach procedure, the Naperian logarithm of the real Fourier coefficient (A(L)) was related to K^2 as follows [17]:

$$\ln A(L) = \ln A_L^S - 2\pi^2 L^2 \varepsilon^2 K^2 \tag{1}$$

In the above equation, A_L^S and ε^2 represent the size Fourier coefficient and the mean square lattice strain generated by dislocations, respectively. K is the length of diffraction vector defined as $K=2\sin(\theta)/\lambda$ where θ is the Bragg angle and λ is the wavelength of the incident beam. For a certain magnitude of L, A_L^S can be calculated from the y-intercept of the above line. This can be repeated for other magnitudes of the Fourier variable, and finally a table of A_L^S values in terms of L is obtained. By plotting A_L^S against L, a curve is obtained. The intersection of the tangent to this curve at the point L=0 with the horizon axis will yield the size parameter, which is interpreted as the subgrain/dislocation cell size in the microstructure [15-18].

3. Results and Discussion

A typical light microscope image taken from the microstructure of AISI 1020 steel after initial annealing treatment is shown in Fig. 1a. In this figure, it is clear that the annealing treatment created an equilibrium microstructure mainly consisting of equiaxed ferrite grains (white areas) along with about 18% of pearlite grains in the steel. The average grain size of ferrite grains was found to be around 34 micrometers. In addition, inclusions are also observed inside some grains. Fig. 1b shows a typical low magnifications TEM image of the microstructure of AISI 1020 steel after applying ECAP for 10 passes. This micrograph shows that the application of heavy plastic strain of ε_{VM} =8 to the starting coarse-grained material strongly reduced its microstructure and created a mixture of equiaxed and elongated grains with a size in the ultrafine range.

The size distribution of the elongated grains was relatively wide and varied from 180 to 700nm. Their average width was about 270nm. Equiaxed grains also had different sizes, and the average size of these grains was 320nm. Inside most grains, the contrast was not uniform and varied from one region to another, indicating the fact that there existed finer microstructural components. Dislocation cells and subgrains were clearly seen inside some grains. In this regard, Fig. 1c exhibits a relatively large grain surrounded by sharp and clear boundaries whose interior was subdivided into five subgrains labeled as 1 to 5.

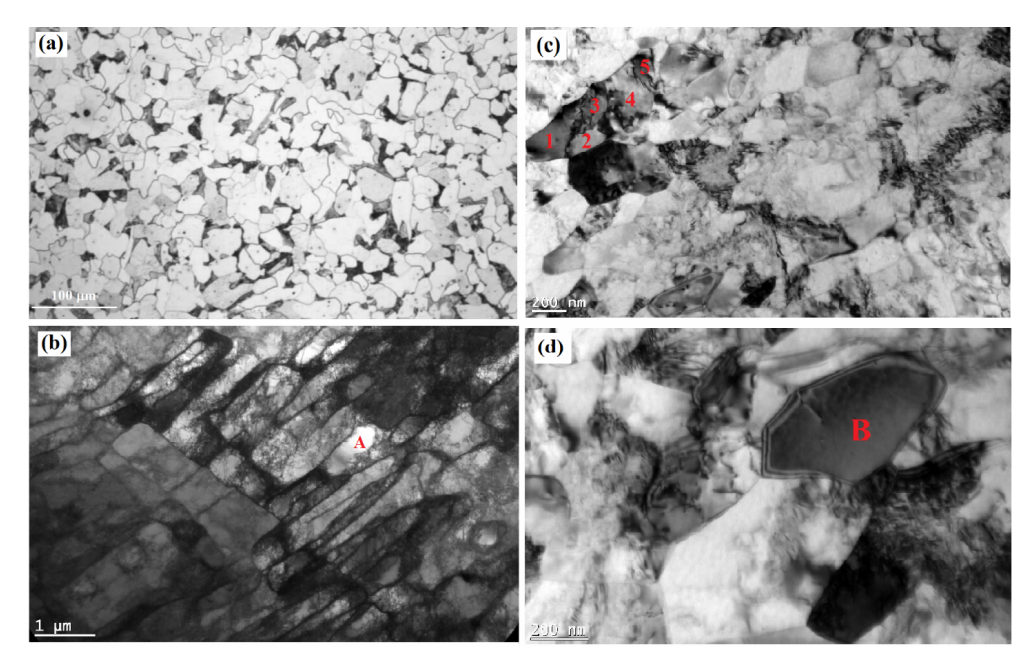


Fig. 1. The results of light and TEM observations for AISI 1020 plain carbon steel: 1a Light microscopy image taken before ECAP, and 1(b, c, d) TEM images taken after processing by 10 passes of ECAP.

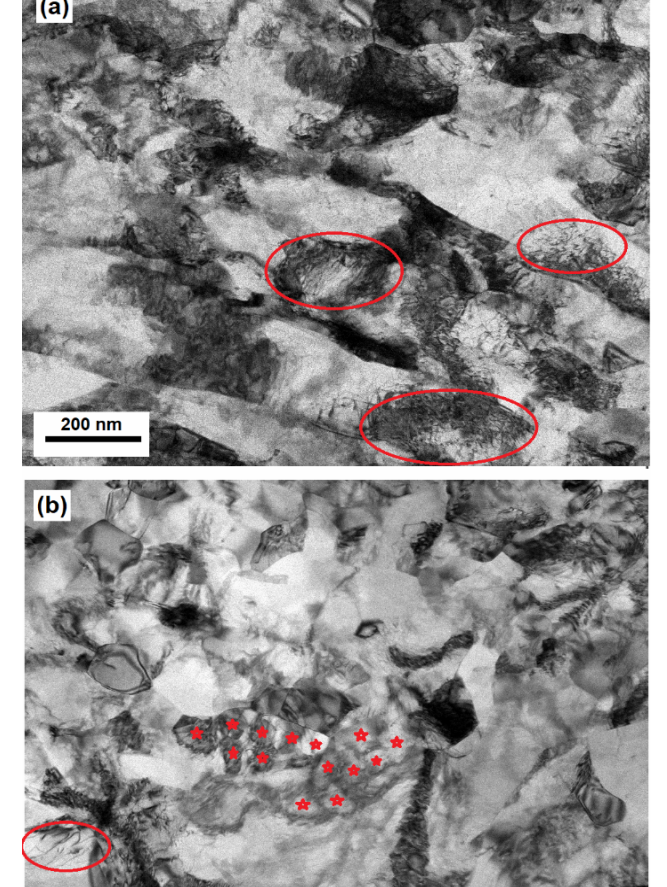


Fig. 2. Bright field TEM micrographs of AISI 1020 plain carbon processed by ECAP for 10 passes taken from the other part of TEM specimen.

500 nm

Most grains contain a high density of dislocations; however, single grains almost free of dislocations can also be found. Examples of these grains are marked with A in Fig. 1b and B in Fig. 1d. The latter is a higher magnification image taken from another region of the same TEM specimen. The appearance of such inhomogeneous microstructure in metals subjected to SPD processing is most common, as discussed in detail in reference [19].

Fig. 2 shows the bright field TEM micrographs taken from the other part of the same TEM specimen. In these micrographs, dislocations whether single or tangled are clearly seen in the regions enclosed by red ellipses. Another obvious feature of the microstructure is the existence of subgrains (the areas marked with red stars in Fig. 2b) which formed inside large grains, subdividing them into smaller parts. These subgrains have dimensions within the range of ~ 100 to ~ 180 nm with a mean size around 151 nm. It will be shown in the rest of the article that the mean subgrain size obtained by TEM observations is in a good agreement with the crystallite size calculated by the X-ray diffraction peak profile analysis.

In face centered cubic (FCC) structural metals with medium to high stacking fault energy (SFE) such Cu and Alas well as in ferritic steels where bcc ferrite has a high stacking fault energy, the grain size refining during SPD processes is carried out by the dislocation-controlled grain subdivision mechanism [4]. Heavy straining introduces a very high dislocation density in the initial coarse-grained material. These dislocations arrange themselves into various configurations such as the incidental dislocation boundaries, geometrically necessary boundaries or dense dislocation walls result-

ing in the formation of dislocation cells or cell blocks typically of the order of several hundred nanometers in size [20]. When deformation is continued to a larger plastic strain, the dislocation cell walls generated during the initial stage of deformation gradually evolve into low energy dislocation configurations and form subgrain low-angle boundaries [4, 5]. Transformation of these boundaries into high-angle ones occur through the absorption of more lattice dislocations from grain interior during further straining [4]; therefore, an ultrafine-grained microstructure is formed within the material.

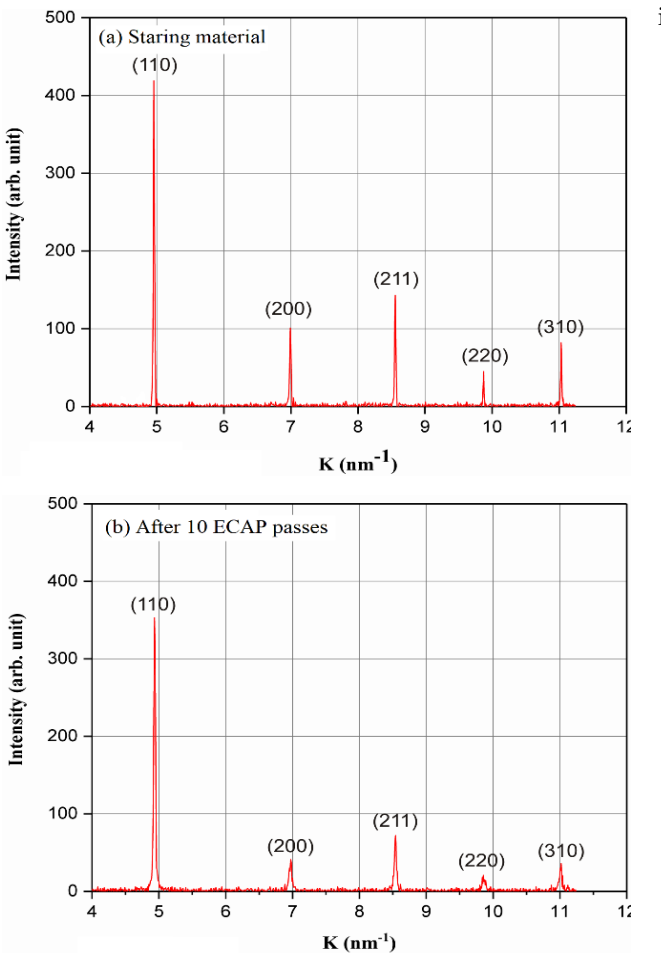


Fig. 3. The X-ray diffraction patterns of AISI 1020 steel before and after deformation by ECAP.

Fig. 3 shows the X-ray diffraction patterns of 1020 steel before and after deformation by ECAP. As shown in the figure, all peaks appeared in both the starting material and that subjected to ECAP are related to alpha iron. It is quite evident that the peak broadening and peak intensity reduction occurred after deformation by ECAP. This finding which is in line with the most previous reports [15-18] could be attributed to a combination of finer grain/subgrain size and higher content of dislocation density of the microstructure obtained by ECAP [16, 18]. Furthermore, it should also be noted that the induced shear deformation by ECAP changes the texture; therefore, the change in the grains'

orientation will also affect the intensity of the peaks [7].

As stated in the Experimental Procedure section, in this research, the peak profile analysis was carried out using Warren-Averbach method. Fig. 4 shows the normalized theoretical profiles based on the Lorentzian and Gaussian functions as well as the average curve fitted to the measured data, for two peaks of the same family of planes (i.e. for (110) and (220) planes) both in the annealed starting material and the sample deformed by ECAP for 10 passes. The broadening of the peaks as a result of plastic deformation induced by ECAP can be clearly seen in these figures, especially in the peak corresponding to the (220) reflection.

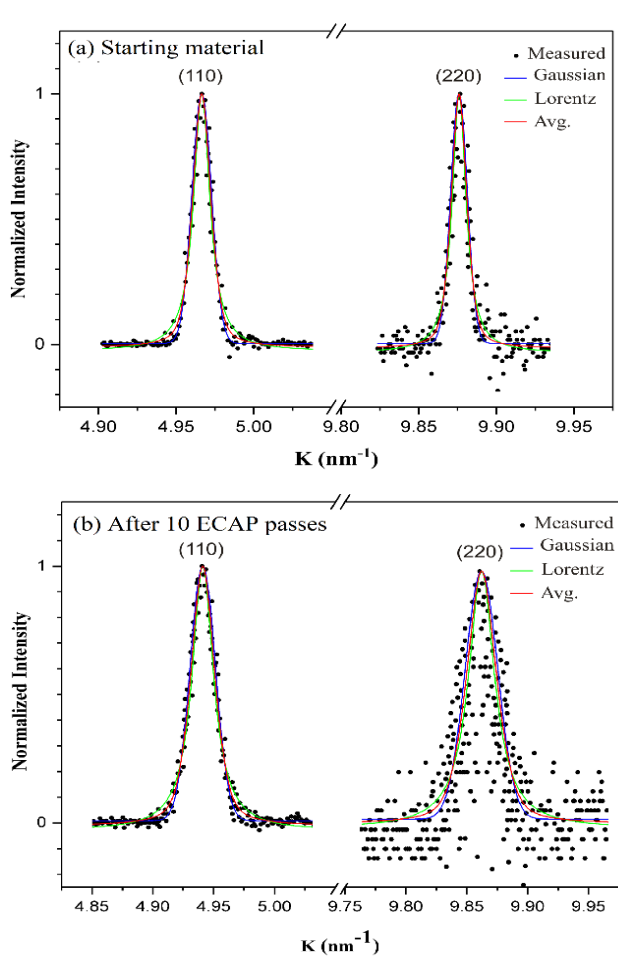


Fig. 4. Theoretical profiles based on the Lorentzian and Gaussian functions fitted to data recorded for two peaks corresponding to (110) and (220) reflections in the starting material and the sample deformed by ECAP for 10 passes.

After preliminary data processing on the diffraction patterns recorded by the diffractometer, entailing elimination of $K\alpha_2$ profiles and background removal, the resultant profile of each peak was estimated by the Gaussian and Lorentzian fitting, and the fit parameters were determined. In the following stage, the location of the peak top in each fitted Gaussian and Lorentzian function was transferred to the origin.

Table 2

Average of normalized FT real part of Gaussian and Lorentzian functions fitted to experimental data collected for two peaks corresponding to (110) and (220) reflections after instrumental broadening removal.

Reflection	FT real part of the theoretical profile fitted to experimental data (A(L))
(110)	$A(L) = \frac{1}{2} \times \exp(-0.00145L^2) + \exp(-0.02746L)$
(220)	$A(L) = \frac{1}{2} \times \left[\exp\left(-0.00385L^2\right) + \exp\left(-0.05139L\right) \right]$

In plain English, zero was substituted for K_C in their equations. After that, these functions were subjected to the Fourier transformation (FT). Then, the

instrumental broadening was eliminated from the profiles of each peak using the following equation [18]:

 $FT\ real\ part\ after\ removing\ the\ instrument-related\ broadenning = \frac{FT\ real\ part\ of\ a\ peak\ in\ deformed\ sample}{FT\ real\ part\ of\ the\ same\ peak\ in\ the\ standard\ specimen}$

For doing this, a well-annealed coarse-grained sample was employed as the standard specimen. After instrumental removing of the Fourier-transformed Gaussian and Lorentzian functions, they were first normalized. This was carried out simply by substituting the number 1 for the coefficient of the exponential part in their expressions. Finally, the resulting expressions were averaged. The result of these calculations is presented in Table 2. These are, in fact, the FT real part of the theoretical profile fitted to experimental data, which will be used thereafter instead of A(L) in Eq. (1).

In the following, A(L) values were calculated from the above expressions for different values of the Fourier variable (L) from zero to 150 and plotted against L for two peaks of (110) and (220) in Fig. 5.

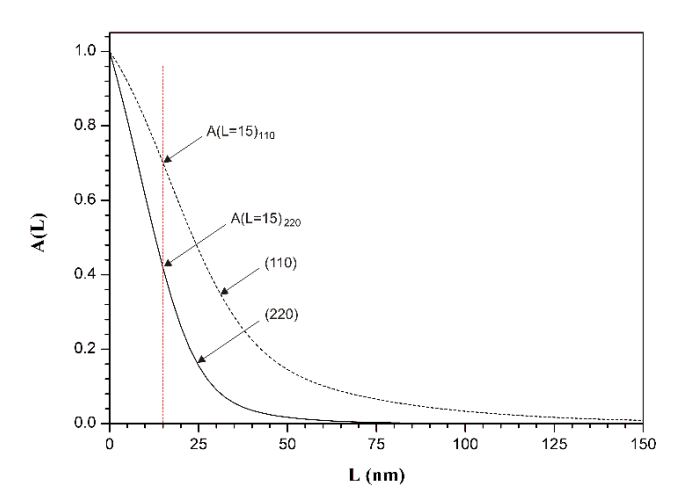


Fig. 5. A(L) versus L plots for two peaks corresponding to (110) and (220) reflections in the sample subjected to ECAP for 10 passes.

After this step, A(L) was determined on each of two peaks for a certain magnitude of L, and then the natural logarithm of A(L) values was plotted as a function of the square of the diffraction vector of the peaks. The size Fourier coefficient (A_L^S) was obtained from the y-intercept of the above line. This mathematical operation was repeated for other values of the Fourier variable, and eventually a table of A_L^S values in terms of L was obtained. The data of the above table was shown as a plot in Fig. 6. The subgrain/dislocation cell size was determined by drawing a tangent line to the curve at the point L=0 and determining its intersection with the horizon axis. As shown in Fig. 6, the size of the subgrains for the 10 passes ECAP-ed sample which was 142.8 nm is in a good agreement with the size of the microstructural components that appeared inside the elongated or equiaxed grains in TEM observations (Fig. 2b).

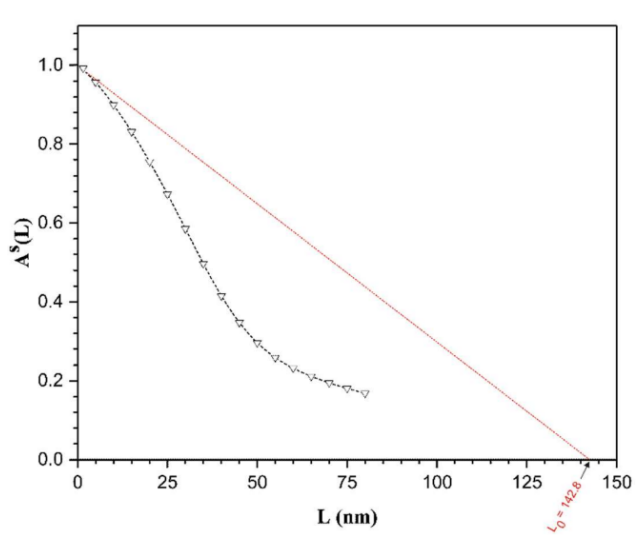


Fig. 6. Size Fourier coefficient (A_L^S) versus Fourier variable (L) plot for AISI 1020 steel processed by ECAP for 10 passes. The intersection of tangent line to the curve at the point L=0 with the horizon axis yielded the subgrain/dislocation cell size.

The effect of ECAP on mechanical properties of 1020 steel was evaluated in this research by tensile testing and microhardness measurements. In this regard, the average Vickers microhardness values are plotted in Fig. 7 against the accumulated equivalent strain imparted into the material by different number of ECAP passes. It is seen that the microhardness increases monotonically from HV=125 for the starting material to HV=395 after 10 passes of ECAP, indicating

a 2.2 times growth. With more a precise look at the plot, it can be understood that the slope of increase in the initial two passes is slightly steeper than the other passes.

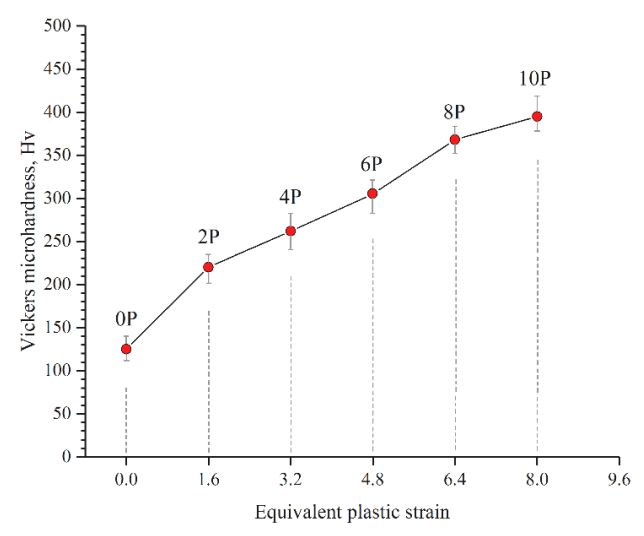


Fig. 7. Plot of average Vickers microhardness values of AISI 1020 steel against the accumulated equivalent strain imparted into the material by different numbers of ECAP passes.

Fig. 8 shows the engineering stress-strain curves of 1020 steel in the initial state and after processing by ECAP. The tensile properties extracted from the stress-strain curves along with the average microhardness values obtained for each processing condition are summarized in Table 3. At first glance, it can be observed that the starting material as well as the sample processed by ECAP for two passes showed the yield point phenomenon during tensile testing, while such behavior is not observed in the other ECAP-ed samples. The next point is the wide range of work hardening in the curve of starting material, a behavior not seen in the samples subjected to ECAP processing. As can be seen, the ECAP-ed specimens exhibited a narrow work hardening range, and then necked rapidly. This behavior can be explained by the low capacity of the UFG microstructure to further work hardening [21]. The ECAP-ed material contains a huge number of dislocations previously generated during a severe deformation; therefore, in spite of the annealed starting material, the ability of the UFG structure to introduce new and more dislocations during tensile testing is very limited [21]. The lack of strain hardening capacity caused premature necking of the UFG microstructure according to the Considère criterion [22].

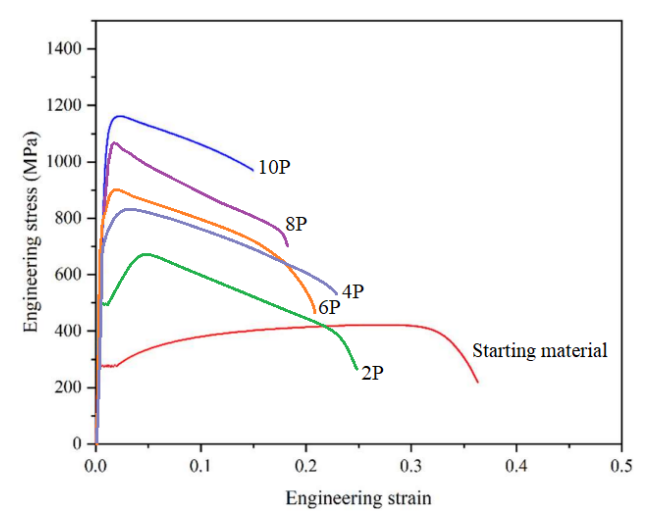


Fig. 8. The engineering stress-strain curves obtained by room temperature tensile testing for AISI 1020 steel before and after deformation by ECAP. 2P, 4P, ..., 10P corresponding to the samples processed by ECAP through 2, 4, ..., and 10 passes, respectively.

It can be seen in Table 3 that the yield strength (YS) and ultimate tensile strength (UTS) of 1020 steel greatly increased after the first two passes and reached 489 and 670MPa, respectively. These strength levels were considerably higher than those measured for the starting material (YS = 280 and UTS = 440MPa). By applying the next passes, the strength increased, but similar to the trend observed previously for microhardness, the slope of the increase was slightly less than the initial passes.

Table 3
Tensile properties and microhardness values of AISI 1020 plain carbon after processing by ECAP for different number of passes.

Processing condition	YS (MPa)	UTS (MPa)	ε_u (%)	ε_f (%)	Microhardness, HV
Starting Material-0P	280^{+18}_{-15}	440^{+31}_{-12}	$30^{+5.2}_{-3}$	$36^{+7}_{-3.4}$	125^{+8}_{-6}
ECAP- 2P	489^{+13}_{-11}	670^{+21}_{-14}	$4.8^{+0.7}_{-0.6}$	$25^{+2.5}_{-1.7}$	220^{+7}_{-13}
ECAP- 4P	735_{-8}^{+12}	820^{+25}_{-19}	$3^{+0.4}_{-0.6}$	$23^{+1.5}_{-2}$	258^{+14}_{-15}
ECAP- 6P	842^{+31}_{-19}	904^{+27}_{-21}	$1.9^{+0.2}_{-0.35}$	$20.8^{+1.1}_{-2}$	305^{+9}_{-17}
ECAP- 8P	990^{+29}_{-34}	1064^{+38}_{-50}	$2.1_{-0.25}^{+0.4}$	$18^{+1.8}_{-2.4}$	367^{+8}_{-10}
ECAP- 10P	1100^{+16}_{-41}	1175_{-56}^{+27}	$2.5^{+.1}_{-0.3}$	$14.8^{+1.4}_{-2.1}$	395^{+20}_{-13}

In general, processing by 10 passes of ECAP strengthened 1020 steel significantly. There was a three times growth in YS from 280MPa to 1100MPa. At the same time, UTS experienced a 167% enhancement from 440MPa to 1175MPa. In contrast to multiple increases observed in the strength and hardness values, 1020 steel experienced a notable decrease (equivalent to 59% loss) in ductility when it was subjected to severe deformation by ECAP. While the elongation to failure of starting material was found as $\varepsilon_f=36\%$, it decreased to 14.8% after applying 10 passes of ECAP. The increase in strength and hardness after ECAP could be attributed to a rise in the dislocation density of material as well as the increase in the fraction of grain/subgrain boundaries as a results of grain refinement occurred during severe plastic deformation. Each of the mentioned factors acted as an obstacle against the movement of dislocations m, making an increase in the necessary external force in order for dislocations to move and cause the subsequent deformation [22].

It is worth noting that according to the study carried out by Shin et al. [7], conducting ECAP on a 0.15wt% C carbon steel at 350°C up to an effective strain of \sim 4 by a die with a channel angle of 90° raised the UTS from 480 to 943MPa (equivalent to 87% enhancement) while ductility experienced a 63% loss from $\varepsilon_f = \sim$ 30 to \sim 11% in total. Comparing the mechanical properties obtained in this research with the results reported by Shin et al. [7] shows that the use of a larger channel angle and, consequently, success in processing safe samples with a higher number of passes, which caused more plastic strain to be imposed to the material, is a successful strategy to achieve higher strengthening with lower ductility loss.

Considering that the grain size of ECAP-ed steel in the research of Shin et al. is almost the same as the mean grain size determined in the current research, the higher strengthening capability may be related to the existence of higher dislocation density and/or smaller size of sub-structures formed in the microstructure. Since the processing temperature in the current research is 50°C lower than that used by Shin et al., it is expected that the recovery will occur in a lower rate, leading to higher dislocation density in the microstructure.

Higher ductility of ECAP-ed material compared to the research of Shin et al. may be explained based on the increase in the fraction of high-angle grain boundaries with increasing accumulated strain and consequently with an increasing role of grain boundary sliding and grain rotations as mechanisms accommodating plastic deformation [5].

The increase in strength caused by ECAP can be due to the contributions from two factors including dislocation strengthening (σ_{ρ}) and boundary strengthening (σ_{b}) . The term (σ_{ρ}) is obtained by the law describing dislocation hardening, which assumes the square

root to be dependent on the dislocation density (ρ) [22]:

$$\sigma_{\rho} = M\alpha G b \rho^{1/2} \tag{3}$$

where M stands the Taylor factor, α is a constant, G represents the shear modulus, and b is the Burgers vector. Kuhlmann-Wilsdorf [23], by assuming that most of the dislocations in the microstructure are present at the sub-boundaries, related dislocation strengthening to the sub-boundary strengthening. Considering that the average spacing between dislocations $(1/\sqrt{\rho})$, which are mostly contained in the cell walls/sub-boundaries, can be related to the dislocation cell /subgrain size Dc by a constant K of value about 10 [23], dislocation cell/subgrain hardening can be described as:

$$\sigma_{\rho} = M\alpha G b \frac{K}{D_C} \tag{4}$$

The term σ_b can be obtained from the Hall–Petch relationship as [22]:

$$\sigma_b = \sigma_0 + kd^{1/2} \tag{5}$$

In the above equation, d is the distance between impenetrable grain boundaries, that is the grain size, σ_0 is friction stress, and k denotes the slope of the straight line relating the yield stress of polycrystalline material to the reciprocal square root of the grain size. Assuming the additive character of these two strengthening mechanisms, the yield stress of the polycrystalline material can be approximated by the following formula:

$$\sigma_y = \sigma_0 + M\alpha Gb \frac{K}{D_C} + kd^{1/2} \tag{6}$$

By substituting the following values: $\sigma_0 = 280 \text{MPa}$, b = 0.250 nm [24], G = 75 GPa [24], M = 2.7 [24], $\alpha = 0.25$ [25], K = 10 [23], k = 15.1 MPa mm^{0.5} [26], and placing the subgrain size and grain size obtained for 10 passes ECAP-ed sample i.e. $D_C = 142.8 \text{nm}$, d = 320 nm, yield stress was approximated to be 2015MPa. This value is $\sim 83\%$ greater than the value measured experimentally (YS = 1100 MPa) for 1020 steel after 10 passes of ECAP.

The reason for the difference can be attributed to the fact that the equation used to include the effect of subgrains on the strengthening is not accurate enough. A more accurate relation was given by Hansen [27], in which the density of dislocations present at subgrain boundaries was connected to subgrain size and with boundary misorientation angle θ . Considering the subgrain boundary area per volume of material as about $3/D_C$ and the dislocation density per boundary area related to the misorientation as θ/b , dislocation cell/subgrain hardening can be described as:

$$\sigma_{\rho} = M\alpha G b \left(\frac{3\theta b}{D_C}\right)^{0.5} \tag{7}$$

In order to use Eq. (7), it is necessary to measure boundary misorientation angle θ by a proper tool such as a scanning electron microscope (SEM) equipped with an electron backscatter diffraction (EBSD) detector. Due to the fact that such type of characterization was not carried out in the present research, it was not possible for us to use Eq. (7) and estimate the yield strength in a more precise way.

The occurrence of the yield point phenomenon in tensile testing of the starting material may be explained as follows. In conventional coarse–grained materials, the yield point phenomenon is usually explained by Cottrell theory in terms of the interaction energy between dislocations and solute atoms [28]. The solute atoms tend to settle in areas with enough open spaces. The grain boundaries provide more open regions than those exist usually under dislocation lines. Due to the extremely fine grain/subgrain structure, the ECAP-ed material is full of boundaries which are placed at close distances. Therefore, solute atoms easily travel these short distances and reach grain boundaries. As a result, most of the solute atoms in severely deformed microstructure segregate in grain/subgrain boundaries instead of dislocation cores [29]. This results in an insufficient number of locked dislocations in the microstructure to make the yield point phenomenon. In contrast, the grain boundaries of the coarse-grained starting material are very far from each other. The solute atoms have little chance of traveling these long distances; therefore, they inevitably try to settle themselves in limited open spaces under the dislocation lines. This makes the dislocations be locked, leading to the yield point phenomenon during the next deformation.

4. Conclusion

In the current research, AISI 1020 plain carbon steel was subjected to 10 passes of ECAP at 300°C and, the microstructure and mechanical properties of the processed material were evaluated and compared with the starting counterpart. The results obtained in the present study led to the following conclusions:

- ECAP proved to be very efficient in refining the microstructure. Direct observations by TEM revealed that by applying 10 ECAP passes, a UFG microstructure with a mixture of equiaxed and elongated grains of 320nm in the mean size and 270nm in width is formed in the steel, respectively.
- 2) X-ray peak profile analysis by the Warren-Averbakh procedure estimated the size of substructures (subgrains/dislocation cells) formed inside main grains as ∼143nm.
- 3) ECAP was demonstrated to be very effective in strengthening of 1020 steel. It caused a three

- times increase in yield strength from 280 MPa to 1100 MPa. At the same time, the steel maintained an acceptable ductility of ε_f =14.8% at this high level of strength.
- 4) In spite of the coarse-grained material, the yield point phenomenon did not occur during tensile testing of ECAP-ed specimens with 10 passes. This behavior was attributed to the presence of a large fraction of closely spaced grain boundaries inside the UFG microstructure.

References

- [1] C. Phelps, Carbon Steel: Microstructure, Mechanical Properties and Applications, Nova Science Pub Inc, 2019.
- [2] C.R. Brooks, Principles of the Heat Treatment Plain Carbon and Alloy Steels, ASM international, 1996.
- [3] J.R. Davis, ASM Specialty Handbook Carbon and Alloy Steels, ASM international, 1996.
- [4] R.Z. Valiev, R.K. Islamgaliev, and I.V. Alexandrov, Bulk nanostructured materials from severe plastic deformation, Prog. Mater. Sci., 45 (2000) 103-189.
- [5] R.Z. Valiev, T.G. Langdon, Principles of equal channel angular pressing as a processing tool for grain refinement, Prog. Mater. Sci., 51 (2006) 881-981.
- [6] R. Song. D. Ponge, D. Raabe, J.G. Speer, D.K. Matlock, Overview of processing, microstructure and mechanical properties of ultrafine grained bcc steels, Mater. Sci. Eng. A, 44(1-2) (2006) 1-17.
- [7] D.H. Shin, Plastic Flow Characteristics of Ultrafine Grained Low Carbon Steel during Tensile Deformation, Met. Mater. Inter. 7(6) (2001) 573-577.
- [8] D.H. Shin, J. Kim, K.T. Park, A New Low Carbon Steel Microstructure: Ultrafine Ferrite Grains with Homogeneously Distributed Fine Cementite Particles, Met. Mater. Inter. 7(5) (2001) 431-535.
- [9] Y. Fukuda, K. Oh-ishi, Z. Horita, T.G. Langdon, Processing of low-carbon steel by equal-channel angular pressing, Acta Mater. 50 (2002) 1359-1368.
- [10] K.T. Park, Y.S. Kim, J.G. Lee, D.H. Shin, Thermal stability and mechanical properties of ultrafine grained low carbon steel, Mater. Sci. Eng. A, 293 (2000) 165-172.

- [11] R.B. Singh, N.K. Mukhopadhyay, G.V.S. Sastry, R. Manna, Recovery of Ductility in Ultrafine-Grained Low-Carbon Steel Processed Through Equal-Channel Angular Pressing Followed by Cold Rolling and Flash Annealing, Metall. Mater. Trans. A, 48(A) (2017) 1189-1203.
- [12] Y.I. Son, Y.K. Lee, K.T. Park, Reverse Transformation of Ferrite and Pearlite to Austenite in an Ultrafine-Grained Low-Carbon Steel Fabricated by Severe Plastic Deformation, Metall. Mater. Trans. A, 37(A) (2006) 3161-3164.
- [13] R.B. Figueiredo, M.T. Paulino Aguilar, P.R. Celtin, Finite element modeling of plastic instability during ECAP processing of flow-softening materials, Mater. Sci. Eng. A 430 (2006) 179–184.
- [14] K. Hajizadeh. K. Topolski, B. Eghbali, K.J. Kurzydlowski, Ultrafine grained bulk CP-Ti processed by multi pass ECAP at warm deformation region, Mater. Chem. Phys. 143(3) (2014) 1032-1038.
- [15] T. Ungar, I. Dragomir, A. Revesz, A. Borbely, J. Appl. Crystallogr. 32 (1999) 992-1002.
- [16] K. Hajizadeh, V. Abbasi, K.J. Kurzydlowski, Insight into dislocation activity during ECAP processing of AISI 304 stainless steel studied by X-ray diffraction profile analysis. J. appl. Phys. A, 128 (2022) 806.
- [17] J. Gubicza, L. Balogh,, R.J. Hellmig, Y. Estrin, T. Ungar, Dislocation structure and crystallite size in severely deformed copper by X-ray peak profile analysis., Mater. Sci. Eng. A, 400-401 (2005) 334-338.
- [18] K. Hajizadeh, H. Farhad, K.J. Kurzydlowski, Effect of ECAP processing routs on the microstructural characteristic of commercial purity titanium, J. appl. Phys. A, 129 (2023) 583.

- [19] T. Zhu, J.Y. Huang, J. Gubicza, T. Ungar, Y.M. Wang, E. Ma, R.Z. Valiev, Nanostructures in Ti processed by severe plastic deformation, J. Mater. Res. 18 (2003) 1908-1917.
- [20] R.D. Doherty, P.B. Prangnell, F.J. Humphreys, Current issues in recrystallization: a review, Mater. Sci. Eng. A, 238 (1997) 219-274.
- [21] Y.M. Wang, E. Ma, Three strategies to achieve uniform tensile deformation in a nanostructured metal, Acta Mater. 52(6) (2003) 1699-1709.
- [22] G.E. Dieter, Mechanical Metallurgy, McGraw Hill, 1998.
- [23] D. Kuhlmann-Wilsdorf, Theory of plastic deformation: properties of low energy dislocation structures, Mater. Sci. Eng. 113A (1989) 1-41.
- [24] J. Duan, D. Farrugiab, C. Davisaand, Z. Li, Effect of impurities on the microstructure and mechanical properties of a lowcarbon steel, IRONMAK-ING & STEELMAKING, 49 (2022) 140-146.
- [25] H. Zheng, G. Liu, S. Tong, G. Su, X. Liang, X. Sun, Optimizing the Strength and Toughness of V/Mo-Modified 0.22C-5.24Mn Steel by Short-Time Partial Austenitization Process, Materials 17(3) (2024) 687.
- [26] J. Kang, Y. Ko Strengthening of 0.18 wt % C Steel by Cold Differential Speed Rolling, Materials 15(10) (2022) 3717.
- [27] N. Hansen, Hall–Petch relation and boundary strengthening, Scripta Mater. 51 (2004) 801-806.
- [28] E.O. Hall, Yield Point Phenomena in Metals and Alloys, Plenum, 1970.
- [29] S. Sauvage, G. wilde, S. divinski, Z. Horita, R.Z. Valiev, Grain boundaries in ultrafine-grained materials processed by severe plastic deformation and related phenomena, Mater. Sci. Eng. A, 540 (2012) 1-12.